NJC

New Journal of Chemistry

A journal for new directions in chemistry

Accepted Manuscript

This article can be cited before page numbers have been issued, to do this please use: S. S. Birajdar, S. N. Naqvi, K. S. More, A. L. Puyad, R. Kumar, S. V. Bhosale and S. V. Bhosale, *New J. Chem.*, 2021, DOI: 10.1039/D0NJ05045H.

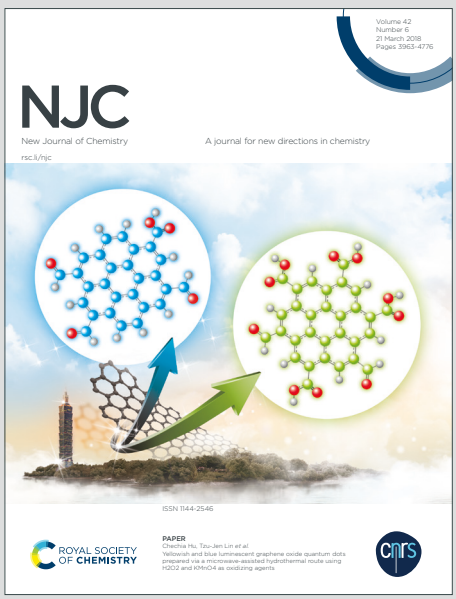

This is an Accepted Manuscript, which has been through the Royal Society of Chemistry peer review process and has been accepted for publication.

Accepted Manuscripts are published online shortly after acceptance, before technical editing, formatting and proof reading. Using this free service, authors can make their results available to the community, in citable form, before we publish the edited article. We will replace this Accepted Manuscript with the edited and formatted Advance Article as soon as it is available.

You can find more information about Accepted Manuscripts in the Information for Authors.

Please note that technical editing may introduce minor changes to the text and/or graphics, which may alter content. The journal's standard Terms & Conditions and the Ethical guidelines still apply. In no event shall the Royal Society of Chemistry be held responsible for any errors or omissions in this Accepted Manuscript or any consequences arising from the use of any information it contains.

View Article Online
DOI: 10.1039/D0NJ05045H

ARTICLE

Influences of number of 2-ethylhexylamine chain substituents on electron transport characteristics of core-substituted naphthalene diimide analogues

Received 00th January 20xx,
Accepted 00th January 20xx

DOI: 10.1039/x0xx00000x

Shailesh S. Birajdar, [a,e,†] Samya Naqvi, [b,†] Kerba S. More,[c] Avinash L. Puyad,[d] Rachana Kumar,* [b,e] Sidhanath V. Bhosale, *[a,e] Sheshanath V. Bhosale*[c]

We designed and synthesized a series naphthalenediimide (NDI) derivatives through core-substitution (coded as: cNDI) with various number of 2-ethyl-hexylamine (EHA) chains at different positions. The molecular structure of cNDI derivatives such as cNDI-1EHA, cNDI-2EHA, cNDI-3EHA and cNDI-4EHA bearing one, two, three and four 2-ethyl-hexylamine chain, respectively is confirmed by different spectroscopic techniques such as FTIR, ^{1}H-NMR, ^{13}C-NMR spectroscopy and Mass spectrometry. Interestingly, incorporation of different numbers of 2-ethyl-hexylamine on electron deficient cNDI yields diverse photophysical and electrochemical properties. The change in number of alkyl chain on NDI core significantly influences the redox properties and highest occupied molecular orbital (HOMO) and lowest unoccupied molecular orbital (LUMO) energy levels. The crystal packing and changes in morphology of the spin coated films before and after annealing are reorganized differently depending on the number of 2-ethyl-hexylamine topology proved by scanning electron microscopy (SEM) and X-ray diffraction (XRD) techniques. The electron mobility of cNDIs were examined following the standard protocol of space-charge limiting current (SCLC) method. The NDI derivatives bearing various number of 2-ethyl-hexylamine chain at NDI core with thermal treatment at 170 ºC exhibits very good electron mobility of the order of 10^{-6} to 10^{-4} cm^2/Vs. The observed electron mobility trends are not only depends on number of 2-ethyl-hexylaminesubstituents but also on the changes in thin-film morphology.

1. Introduction

Development of air-stable organic semiconductor materials have attracted considerable attention for their potential application as active layers or transport layer for flexible and large-area organic electronics, organic light emitting diodes (OLEDs), bipolar transistors, printed circuits, electronic papers, optoelectronic sensors, organic solar cells and so on.[1-8] To fabricate p- and n-type semiconducting material various π-conjugated chromophores have been designed and synthesized. Literature search revealed that development of n-type organic electron-transport material lags far behind to that of p-type semiconductors due to their instability, inferior performance and few other affairs.[9-12] Many of the n-type organic semiconductors (OSCs) exhibiting the limited structural diversity, sensitivity to moisture, oxygen or light and device performances.[13,14] The n-type materials must exhibit strong intermolecular π-π staking interaction in the solid state to facilitate high electron mobility.[15] The stability of n-type OSCs is affected by the reasonably less deeper LUMO energy levels.[16]Therefore, development of air-stable novel high-performance n-type OSCs have become an important task for the researchers and to overcome these limitations enormous efforts have been dedicated to design and synthesize air-stable n-type OSCs with low-lying LUMO.[17,18] It was found that to address this issue, various n-type OSCs have been designed and synthesized such as fullerene derivatives,[19,20] benzothiadiazole,[21,22] diketopyrrolopyrrole,[23,24] isoindigo,[25,26] bisthienoistain,[27] rylene dyes,[28,29] 7,7,8,8,-tetraycanoquinodimethane (TCNQ)[30] etc. These building blocks are used in small molecule semiconductors as well as in polymers.

Recently, rylene diimide chromophores such as pyromelliticdiimides (PyDIs), naphthalenediimide (NDIs), core-substituted NDIs, and perylenediimides (PDIs) have been

[a.] Polymers and Functional Materials Division, CSIR-Indian Institute of Chemical Technology, Hyderabad-500007, Telangana, India. Email: bhosale@iict.res.in
[b.] Advanced Materials and Devices Metrology Division, Photovoltaic Metrology Group, CSIR-National Physical Laboratory, Dr. K. S. Krishnan Marg, New Delhi 110012, India E-mail: rachanak.npl@nic.in ; rachanasinghchem@gmail.com
[c.] School of Chemical Sciences, Goa University, Taleigao Plateau, Goa-403206, India E-mail: svbhosale@unigoa.ac.in
[d.] School of Chemical Sciences, Swami Ramanand Teerth Marathwada University, Nanded 431606, Maharashtra, India.
[e.] Academy of Scientific and Innovative Research (AcSIR), Ghaziabad- 201002, Uttar Pradesh, India
† First two authors contributed equally
Electronic Supplementary Information (ESI) available: [Scheme S1, FT-IR, ^{1}H NMR, ^{13}C NMR spectra and Mass & HRMS spectrum, XRD spectra, SEM images, experimental conditions and device architecture with electron mobility properties, DFT and TA-DFT calculations as well as theoretical absorption spectra available]. See DOI: 10.1039/x0xx00000x

DOI: 10.1039/D0NJ05045H

extensively employed to fabricate efficient n-type electron-transporting materials.[28,31,32,33,34,35] Among these building blocks, cNDIs are planar π-conjugated chromophores and have been explored as promising n-type OSCs.[32,34,36,37,38,39,40]In order to apply the NDI chromophores to device applications, much efforts have been devoted to tune their optical, photophysical, electrochemical and electronic properties by modulating at the imide-/core- positions with π-conjugated systems, electron withdrawing groups and alkyl chains.[41,42,43] Moreover, when core of the NDI is modified by a strong electron withdrawing group, one can further lower the LUMO energy levels to increase the air-stability of n-type materials and facilitate the electron transport properties.[44-47] The incorporation of alkyl chain at nitrogen atom of the imide enabled smooth solution processability and self-assembly due to good solubility.[42,48,49] Sauvé group demonstrated that the NDI functionalization at core tuned the optoelectronic properties of the chromophore and their applications in non-fullerene solar cells.[50] On the basis of imide-/core-substitution strategy a series of novel NDI based small molecules and polymers have been explored as n-type semiconductor with high electron mobility under inert atmosphere and under vacuum was achieved.[51] Moreover, it is notable that there are very few examples have been reported in the literature in which how the modification of the side chain structure, length, and branching significantly influences the solubility, packing structure and performance of the carrier mobility device. Nevertheless, Ma *et al.* have reported the first time effect of alkyl chain length on stacking and charge transfer mobility and also demonstrated that the short alkyl chain at the diimide position of the NDI and shown to be useful for charge transport.[52] Furthermore, McNeill and co-workers demonstrated the effect of alkyl side-chain substituent and length on the thin-film morphology and solution processed NDI chromophores OFETs device performance.[53] However, to the best of our knowledge, the number of alkyl chain and position of substitution at core of the NDI followed by their n-type semiconducting properties are not investigated till to date.

Herein, we investigate the influence of the number of alkyl i.e. 2-ethyl-hexaylamine chain substitution and their position at core of the NDI over electrochemical and electron transport properties. Typically, we have synthesized a series of NDI-based chromophores i.e. cNDI-1EHA, cNDI-2EHA, cNDI-3EHA and cNDI-4EHA, which is substitution at the core with one, two, three and four 2-ethyl-hexylamine chains, respectively (FIg. 1). The optical and electrochemical properties evaluated by means of UV-vis and cyclic voltammetry, respectively. The thin-film morphology is studied by employing SEM and XRD techniques. The structure-property relation has been investigated at different temperatures to enable the effect of temperature and the numbers of 2-ethyl-hexylamine chain on thin-film morphology, electrical conductivity and electron mobility of NDIs. The charge transport properties were calculated using space-charge limiting current (SCLC) model by fabricating electron-only devices. The best performance was produced NDI bearing three 2-ethyl-hexylamine chain i.e., cNDI-3EHA exhibits the maximum electron mobility of 2.69×10^{-4} $cm^2V^{-1}s^{-1}$.

2. Experimental Section

2.1. Thermogravimetric Analysis: Thermogravimetric analysis (TGA) measurement was performed using a TA instruments Q500 TGA under flowing nitrogen gas at a heating rate of 10°C per minute up to 800°C.

2.2. UV-vis Measurements for Solution: UV-vis absorption measurements were performed on UV-vis-1800 Shimadzu spectrometer using 1 cm path length quartz cuvette. A 300 µL aliquot of NDI-1EHA, NDI-1EHA, NDI-2EHA, NDI-3EHA and NDI-4EHA (1×10^{-3} M stock solution) were transferred to a vial and made up to a final volume of 3 mL (1×10^{-4} M) in dichloromethane. The solutions were allowed to equilibrate for 2h prior to their spectral measurements. For thin film measurements, samples were prepared using spin coating method.

2.3. Cyclic Voltammetry Measurements: The solutions of NDI-1EHA, NDI-1EHA, NDI-2EHA, NDI-3EHA and NDI-4EHA and ferrocene (Fc) in dichloromethane were deoxygenated by bubbling nitrogen gas. The electrolyte tetra-n-butylammonium hexafluorophosphate (0.1 M) was used as supporting electrolyte. The CV measurements were performed at room temperature by using a Power Lab ML160 potentiostat interfaced via a Power Lab4/20 controller to a PC running E-Chem for Windows version 1.5.2. Cyclic voltammograms. Platinum is used as a working electrode with saturated calomel electrode (SCE) is a reference electrode, auxiliary electrode: Pt wire. Fc was used as the internal reference; scan rates: 0.100 mV/s, at 20 °C.

2.4. Scanning Electron Microscopy (SEM) Measurements: Firstly, the silicon wafer substrate was cleaned by rising in acetone and ethanol then Milli Q water. Then the sample sputter was coated with gold for 10 s at 0.016 mA Ar plasma (SPI, West Chester, USA) using a FEI Nova NanoSEM (Hillsboro, USA) operating at high vacuum which provided direct visualization of the material. The samples were prepared by solvent evaporation and spin coating methods.

2.5. X-ray Diffraction Measurements: The NDI-1EHA, NDI-1EHA, NDI-2EHA, NDI-3EHA and NDI-4EHA in the DCM solvent mixtures were used for XRD measurements. Then precipitates of NDI-EHAs were dropped on the silicon wafer and dried at 40 oC for 4 h, this process was repeated for 3 times. The thin film of NDI-EHAs was prepared using spin coating techniques. Structure and crystallinity were analysed on a X'Pert PRO PAN alytical machine with a 0.15405 nm Cu-Kα radiation source.

2.6. Device Fabrication

2.6.1. Electron Transport Studies:[41,49,60] The charge carrier mobility of all the materials was investigated by fabricating electron only device. The ITO coated glass substrates were ultrasonically cleaned with soap solution, acetone, isopropyl

alcohol for 10 minutes and dried in a vacuum oven. The zinc oxide (ZnO) precursor solution was spin coated on cleaned ITO substrates and then baked on hot plate at 250 °C for 30 minutes. The active layer solution of all the NDI materials (40 mg/mL) in chlorobenzene was spin-coated on top of ZnO coated ITO substrate with annealing at 170 °C for 15 minutes. Finally, the substrates were loaded into a thermal evaporator for the deposition of the metal electrode, i.e., a 100 nm Al layer was deposited on top of the NDI layer under high vacuum. The I–V characteristics were tested at room temperature under dark condition using a computer controlled Keithley 2420 source measure unit.

3. Results and Discussion

Fig.1 Chemical structures of the naphthalenediimide derivatives cNDI-1EHA, cNDI-2EHA, cNDI-3EHA and cNDI-4EHA.

3.1. Development and synthesis of NDI based molecular architectures

Two known derivatives cNDI-1EHA and cNDI-2EHA were prepared from 1,4,5,8-naphthalene dianhydride in three steps following reported literature procedure (see ESI Scheme S1).[54a] Interestingly to quote here, this is first time we were able to synthesize tri-bromo along with tetra-bromo substituted 1,4,5,8-naphthalene dianhydride (NDA), typically, we obtained compounds NDA-3Br and NDA-4Br[54b] by reacting NDA with dibromohydantoin (DBH) in concentrated sulphuric acid (H_2SO_4) at 90 °C (Scheme 1).

The synthesis of compounds NDI-3Br and NDI-4Br were achieved by the two step reaction sequence via the amide bearing bromo-substituted naphthalene-dicarboxylic acids**1** and **2**. Thus, the reaction of NDA-3Br and NDA-4Br with 2-ethyl-1-hexylamine in acetic acid at 90 °C gave the corresponding products **1** and **2**(Scheme 1). Subsequent reaction of compounds **1** and **2**with phosphorus tribromide (PBr_3) in toluene at reflux temperature gave two products in various proportions i.e. NDI-3Br (20% yield) and NDI-4Br (60% yield) depending on the reaction conditions (see the experimental section). Compound NDI-3Br is a golden yellow solid. ^{1}H NMR spectra indicated the existence of single NDI-Ar proton peak signal at δ 9.00 ppm (FIg. S2). ^{13}C NMR pointed the bromine substituted NDI-Ar carbon (three) peaks at δ 128.40 ppm, 127.78 ppm and 125.31 ppm, whereas, peak at δ 139.20 ppm, which corresponds to the NDI-Ar-H carbon (FIg. S3). Compound NDI-4Br is a dark yellow solid. ^{1}H NMR spectra showed the absence of NDI-Ar peak in aromatic region (FIg. S4).

Furthermore, the synthesis of core-substitution of NDI-3Br and NDI-4Br with 2-ethyl-hexylamine was performed as a nucleophilic substitution reaction at 140 °C for 15 h and 18 h, respectively, to produce cNDI-3EHA and cNDI-4EHA as illustrated in Scheme 1. Compound cNDI-3EHA is a blood red sticky liquid. The FT-IR spectra of compound cNDI-3EHA was measured and displayed in Fig. S14. As illustrated in Fig. S14, the absorption peak appeared at 1637 cm^{-1} is ascribed to imide carbonyl group stretching vibrations and those located at 1281 cm^{-1} is corresponding to C-O stretching vibrations. The absorption peak located at 3450 cm^{-1} is ascribed to N-H stretching vibrations. As seen in Fig. S14, the stretching vibration frequency of C-H exhibit peaks at 2864 cm^{-1} and 2952 cm^{-1}. ^{1}H/^{13}C NMR spectra displayed the existence of peak at δ 7.77 ppm/126.25 ppm, which corresponds to the NDI-Ar hydrogen and carbon atoms, respectively (FIg. S15/S16). MALDI-TOF spectrometry gave m/z peaks at 871.56 $[M+H]^+$ (FIg. S17). Chromophore cNDI-4EHA is a dark green sticky liquid. ^{1}H NMR spectra of cNDI-4EHA does not exhibits any aromatic proton peak (FIg. S19) and in MALDI-TOF spectrum m/z peak at 998.61 corresponds to $[M]^+$ ion (FIg. S21) appeared confirms the formation of complete core nucleophilic substitution. All the synthesized compounds i.e., cNDI-1EHA, cNDI-2EHA, cNDI-3EHA and cNDI-4EHA were utilized for further thermal, optical, electrochemical characterization and device fabrication.

Chen *et.al*., have reported core substituted tetraamino-NDI showing high HOMO and LUMO energy levels and behaving more like electron donor. However, in the present work, all the four NDIs show comparatively deeper HOMO and LUMO energy levels as required for stable n-type OSCs.[42,49]

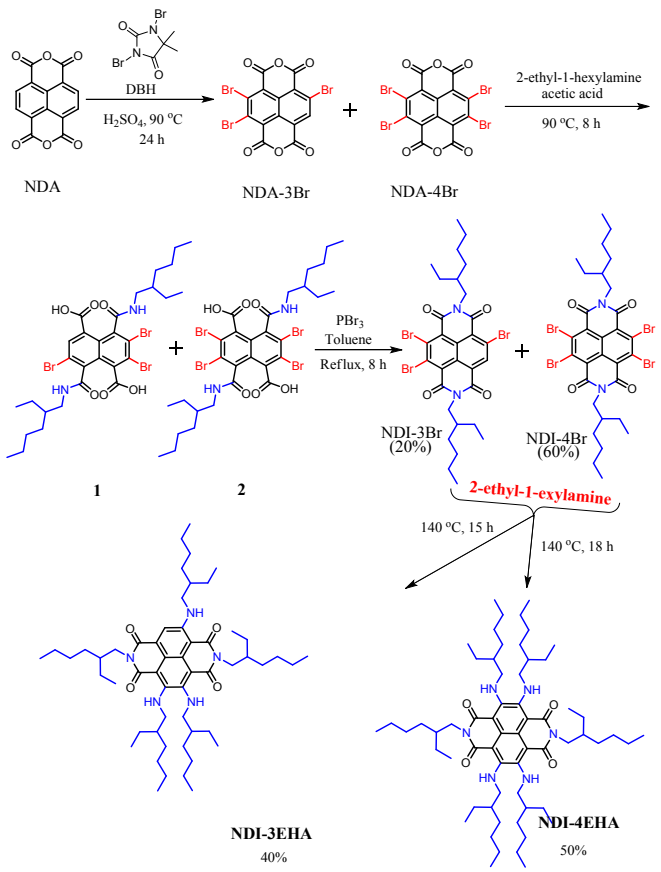

Scheme 1. Synthesis of NDI-3Br, NDI-4Br-cNDI-3EHA and cNDI-4EHA.

3.2. Thermal stability

The thermogravimetric analysis (TGA) experiments were performed under nitrogen atmosphere, in the temperature range from 25 ºC to 800 ºC, at a heating rate of 10 ºC/min. The thermal stability and decomposition behaviour of cNDI-1EHA, cNDI-2EHA, cNDI-3EHA and cNDI-4EHA are illustrated in Flg. 2a, b, c and d, respectively. The 5% weight loss of cNDI-1EHA, cNDI-2EHA, cNDI-3EHA and cNDI-4EHA was observed at 326 ºC, 342 ºC, 311 ºC and 275 ºC, respectively. The thermal decomposition of cNDI-1EHA was observed with a maximum decomposition rate at 400 ºC (with mass loss of 100%) (Flg. 2a, red line). In the case of cNDI-2EHA, the maximum rate decomposition at 410 ºC (90%) was observed (Flg. 2b, blue line). TGA measurements confirmed the decomposition maximum rate at 450 ºC (100%) and 410 ºC (80%) for cNDI-3EHA (Flg. 2c, green line) and cNDI-4EHA (Flg. 2d, black line), respectively. These TGA results suggest that NDI materials cNDI-1EHA, cNDI-2EHA, cNDI-3EHA and cNDI-4EHA are thermally stable and can be utilized at higher annealing temperature for device fabrication.

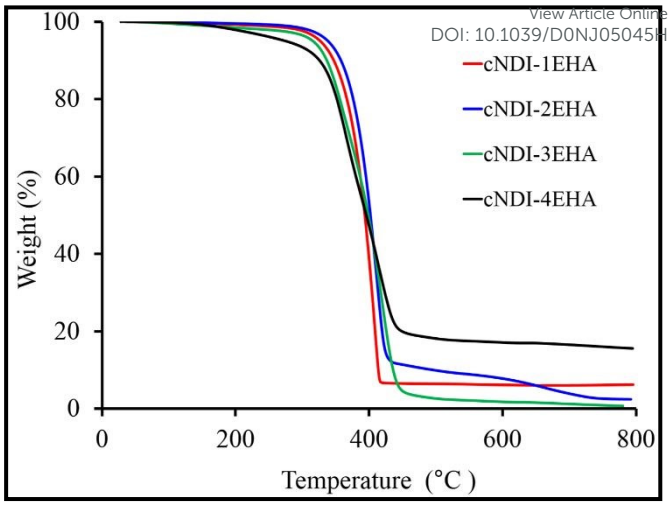

Fig. 2 Thermogravimetric analysis (TGA) of (a) cNDI-1EHA (red line), (b) cNDI-2EHA (blue line), (c) cNDI-3EHA (green line) and (4) cNDI-4EHA (black line).

3.4. Photophysical properties

The UV-vis absorption properties of cNDI-1EHA, cNDI-2EHA, cNDI-3EHA and cNDI-4EHA were studied in dichloromethane (DCM) solution (1.0×10^{-4} M), a solvent of moderate polarity (Flg. 3a), and also in thin-film form (Flg. 3b). The absorption data are summarized in Table 1. cNDI-1EHA has two absorption bands at λ_{max} = 500 nm (shoulder) and 532 nm ($\varepsilon = 1.06 \times 10^{-4}$ $M^{-1}cm^{-1}$). The UV-vis absorption of cNDI-2EHA shows three small absorption peaks at 420 nm($\varepsilon = 0.68 \times 10^{-4}$ $M^{-1}cm^{-1}$), 433 nm($\varepsilon = 0.67 \times 10^{-4}$ $M^{-1}cm^{-1}$), 470 nm ($\varepsilon = 0.67 \times 10^{-4}$ $M^{-1}cm^{-1}$) and one shoulder band at 566 nm ($\varepsilon = 1.43 \times 10^{-4}$ $M^{-1}cm^{-1}$) along with strong peak at 603 nm($\varepsilon = 2.31 \times 10^{-4}$ $M^{-1}cm^{-1}$). cNDI-3EHA display an absorption maximum at around 624 nm ($\varepsilon = 3.26 \times 10^{-4}$ $M^{-1}cm^{-1}$) with shoulder band at 578 nm($\varepsilon = 1.73 \times 10^{-4}$ $M^{-1}cm^{-1}$). The UV-vis absorption spectra of cNDI-4EHA exhibit at 434 nm (shoulder)($\varepsilon = 0.65 \times 10^{-4}$ $M^{-1}cm^{-1}$), 460 nm ($\varepsilon = 0.86 \times 10^{-4}$ $M^{-1}cm^{-1}$) and prominent peak at 651 nm($\varepsilon = 2.26 \times 10^{-4}$ $M^{-1}cm^{-1}$). In DCM solvent, cNDI-1EHA, cNDI-2EHA, cNDI-3EHA and cNDI-4EHA show strong absorption from 400 nm to 730 nm, which is attributed to the intramolecular charge transfer (ICT) transitions from the 2-ethyl-1-hexylamine substituent to NDI ring system. The photoabsorption band of cNDI-2EHA, cNDI-3EHA and cNDI-4EHA shows pronounced bathochromic shift of 78 nm, 94 nm and 121 nm, respectively, as compared to the absorption band of NDI-1EHA appeared at 530 nm (Flg. 3a). This red-shift in absorption peak is due to the increase in number of 2-ethyl-1-hexylamine chain at NDI core leading to the strong ICT excitation. For solid state UV-vis absorption study, thin-film of the NDIs were deposited *via* spin coating on glass substrate. The UV-vis absorption of NDI-1EHA exhibits absorption peaks at 466 nm (shoulder), 505 nm and 532 nm. NDI-2EHA has three small absorption bands at 412 nm, 439 nm and 468 nm along with one broad shoulder peak at 564 nm and a strong band appeared at 600 nm. cNDI-3EHA show an absorption peaks at 538 nm (broad shoulder) and two strong peaks at 578 nm and 614 nm. The spectral absorptions of the cNDI-4EHA appeared at 434 nm (small shoulder), 468 nm (small), broad shoulder at 595 nm and strong band at 645 nm. As illustrated in Flg. 3b, the broadening

View Article Online
DOI: 10.1039/D0NJ05045H

of absorption peaks in thin-films of cNDI-1EHA, cNDI-2EHA, cNDI-3EHA and cNDI-4EHAis attributed to the strong intermolecular interactions and conformational adjustment of the chromophores in thin-film formation. The Thin film spectra were utilized for band gap calculations. The onset of absorption (λ_{max}^{onset} in thin-film) for cNDI-1EHA, cNDI-2EHA, cNDI-3EHA and cNDI-4EHA at λ = 574 nm, 642 nm, 670 nm and 703 nm determines the optical band gap as 2.16 eV, 1.93 eV, 1.85 eV and 1.76 eV, respectively. This suggests that increase in number of 2-ethyl-1-hexylamine substituent at NDI core exhibits longer λ_{max}^{onset} going from cNDI-1EHA, cNDI-2EHA, cNDI-3EHA and cNDI-4EHA and displays strong ICT transition, suggesting significant decrease in optical band gap.

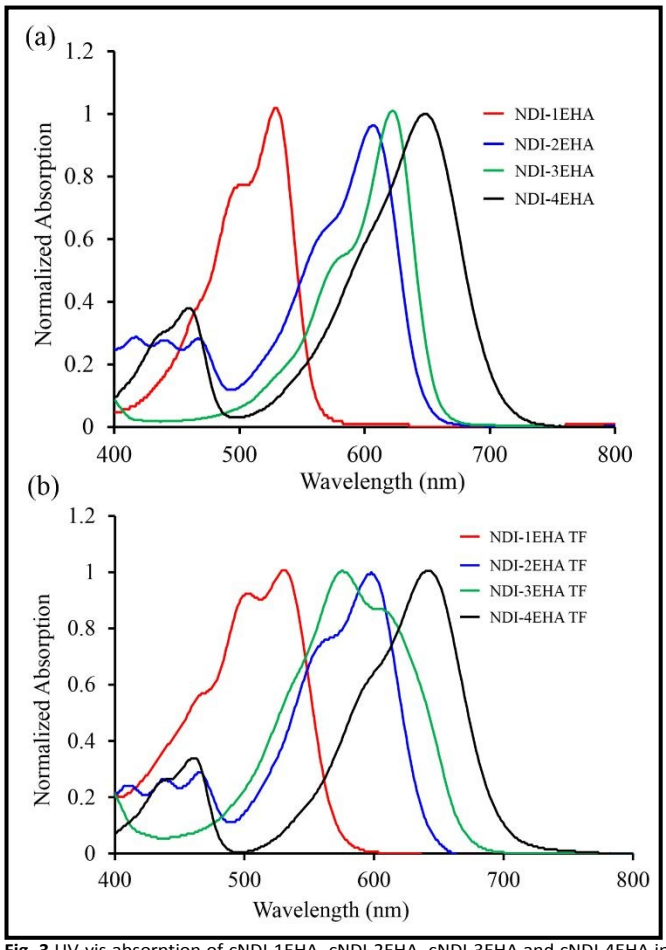

Fig. 3 UV-vis absorption of cNDI-1EHA, cNDI-2EHA, cNDI-3EHA and cNDI-4EHA in (a) DCM solution (1×10^{-4} M) and (b) in spin coated thin-films.

3.5. Electrochemical properties

The electrochemical properties of the cNDI-1EHA, cNDI-2EHA, cNDI-3EHA and cNDI-4EHA were evaluated using cyclic voltammetry (CV). The cyclic voltammetry properties were recorded with saturated calomel electrode (SCE) reference electrode in anhydrous dichloromethane with 0.1 M tetrabutylammonium perchlorate (TBAP) electrolyte at a scan rate of 100 mV/s under nitrogen atmosphere. As illustrated in Fig. 4a, 4b, 4c and 4d and summarized in Table 1, the electrochemical potentials were determined from the onset of the oxidation. The electrochemical parameters of cNDI-1EHA, cNDI-2EHA, cNDI-3EHA and cNDI-4EHA are summarized in Table 1. As shown in Fig. 4a, cNDI-1EHA, cNDI-2EHA, cNDI-3EHA and cNDI-4EHA exhibited multiple irreversible redox peaks as illustrated in Fig. 4a, 4b, 4c and 4d, respectively. The onset oxidation of cNDI-1EHA has one oxidation peak with an E^{ox}_{onset} potential at 0.80 V. NDI-2EHA displays one onset oxidative peak at 0.94 V. The onset oxidative peaks for NDI-3EHA and NDI-4EHA were appeared at 0.80 V and 0.90 V, respectively. The HOMO energy level for the four chromophores cNDI-1EHA, cNDI-2EHA, cNDI-3EHA and cNDI-4EHA were estimated from the onset oxidation potential (E^{ox}_{onset}) by assuming the absolute HOMO energy level of ferrocene to be -4.4 eV as shown in equation 1.

$$E_{HOMO} = - (E^{ox}_{onset} + 4.4)\ eV \quad (1)$$

The calculated HOMO energy level for cNDI-1EHA, cNDI-2EHA, cNDI-3EHA and cNDI-4EHA are -5.20 eV, -5.34 eV, -5.20 eV and -5.20 eV, respectively.

The LUMO energy levels of NDI-1EHA, NDI-2EHA, NDI-3EHA and NDI-4EHA were estimated from equation 2 using onset reduction values -1.00 V, -0.94 V, -1.06 V and -1.00 V, respectively.

$$E_{LUMO} = - (E^{red}_{onset} + 4.4)\ eV \quad (2)$$

The LUMO energy level of cNDI-1EHA, cNDI-2EHA, cNDI-3EHA and cNDI-4EHA are estimated to be -3.40 eV, -3.45 eV, -3.34 eV and -3.42 eV, respectively. The LUMO energy level of cNDI-3EHA (-3.34 eV) is higher than that of the cNDI-1EHA (-3.40 eV) cNDI-2EHA (-3.45 eV) and cNDI-4EHA (-3.42 eV). The calculated band gap for cNDI-1EHA, cNDI-2EHA, cNDI-3EHA and cNDI-4EHA are 1.80 eV, 1.90 eV, 1.86 eV and 1.80 eV, respectively. Such chromophores are potential material for optoelectronic applications.

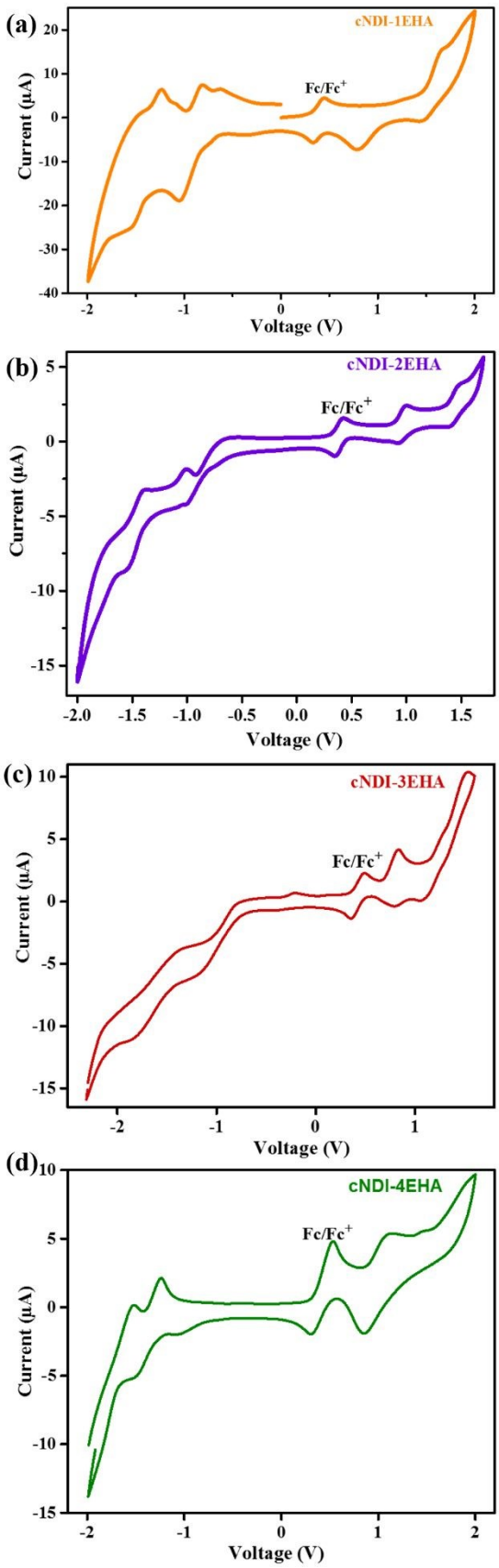

Fig. 4 Cyclic voltammograms of (a) cNDI-1EHA; (b) cNDI-2EHA; (c) cNDI-3EHAand (d) cNDI-4EHA and ferrocene (Fc); in dichloromethane(DCM)solutions containing 0.10 M Bu4NPF6 as supporting electrolyte and platinum as a working electrode with saturated calomel electrode (SCE) is a reference electrode. Fc was used as the internal reference; scan rates: 0.100 mV/s, at 20 °C.

Table 1. Absorption (UV-vis) and electrochemical (CV) properties of cNDI-1EHA, cNDI-2EHA, cNDI-3EHA and cNDI-4EHA.

Molecular Structure/Code	NDI-1EHA	NDI-2EHA	NDI-3EHA	NDI-4EHA
λ_{max} in solution (nm)	500 (shoulder), 528	418, 440, 470, 564 (shoulder) 606	578 (shoulder) , 622	434 (shoulder), 460, 648
λ_{max} in Thin Film (nm)	530	598	607	642
Thin film λ_{max}^{onset} (nm)	574	642	670	703
$E^{opt}g$ (eV)	2.16	1.93	1.85	1.76
E^{ox}_{onset} (V)	0.80	0.94	0.80	0.90
E^{red}_{onset} (V)	-1.00	-0.94	-1.06	-1.00
HOMO (eV)	-5.20	-5.34	-5.20	-5.30
LUMO (eV)	-3.40	-3.45	-3.34	-3.42
$E^{el}g$ (ev)[c]	1.80	1.89	1.86	1.88

λ_{max}: The absorption maxima from the UV–vis spectra in $CHCl_3$ solution or in thin film.
E^{opt}_g : optical band gap determined from the absorption onset in thin film.
$E^{el}g$ (ev) : electrochemical band gap determined from cyclic voltammetry.

3.6. Computational study

To investigate the computational UV-vis and electronic properties of the compounds cNDI-1EHA, cNDI-2EHA, cNDI-3EHA and cNDI-4EHA, density functional theory (DFT) calculations were used. The results of the calculations reported in this work have been obtained using the Gaussian 09*ab initio*/DFT quantum chemical simulation package.[55]The geometry optimization of molecules in the series cNDI-1EHA, cNDI-2EHA, cNDI-3EHA and cNDI-4EHA have been carried out at B3LYP/6-31G* level.In order to confirm the minima, frequency calculations also have been carried out at the same level. Further the geometries of cNDI-1EHA, cNDI-2EHA, cNDI-3EHA and cNDI-4EHA obtained at B3LYP/6-31G* level were subjected to time-dependent density functional theory (TD-DFT) studies using B3LYP/6-31G* level for charge transfer excitations. TD-DFT results were analyzed by employing Gauss-Sum 2.2.5 program,[56] TD-DFT results obtained are illustrated in FIg. S22 and summarized in Table S2. From the TD-DFT results it is seen that absorption trend matches with the UV-vis absorption of cNDI-1EHA, cNDI-2EHA, cNDI-3EHA and cNDI-4EHA in spin coated thin-film form (FIg. 3b). The frontier molecular orbitals (FMO) are generated by using Avogadro[57,58]and are shown in FIg. 5. cNDI-1EHA, cNDI-2EHA, cNDI-3EHA and cNDI-4EHA commonly showed fully delocalised HOMOs and LUMOs across the NDI molecular backbone. As the number of -2ethylhexyl chain substitution increased, the HOMO and LUMO energy levels decreased, in agreement with the electrochemical CV results. The calculated energy band gaps of cNDI-1EHA, cNDI-2EHA, cNDI-3EHA and cNDI-4EHA are 2.939 eV, 2.445 eV, 2.505 eV and 2.282 eV, respectively. The energy band gap decreased slightly from cNDI-1EHA (2.939 eV) to cNDI-4EHA (2.282 eV). Whereas, the E_g cNDI-3EHA (2.505 eV) is slightly higher than that of cNDI-2EHA 92.445 eV). This decrease in energy band gap trend from cNDI-1EHA to cNDI-4EHA is similar to the results

obtained from the absorption measurements (Table 1). But the calculated energy band gap values differ from the E_g^{opt}. This disagreement in energy band gap values were attributed to the DFT calculation of isolated molecules in the gas phase, whereas the UV-vis absorption characteristics were affected by intermolecular interactions *via* π-π staking interactions in the solid state

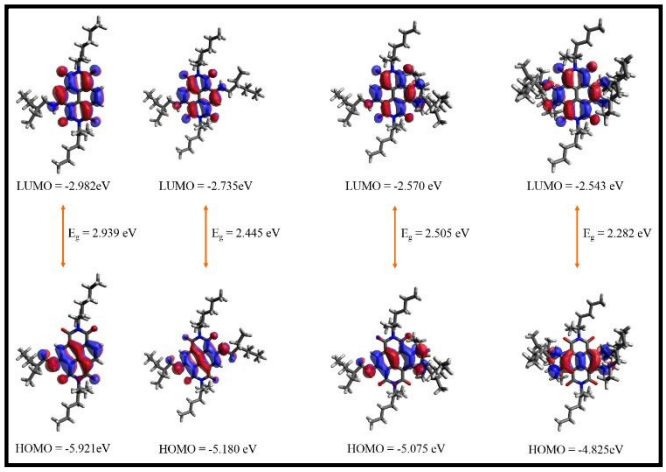

Fig. 5 Frontier molecular orbitals ofcNDI-1EHA, cNDI-2EHA, cNDI-3EHA and cNDI-4EHA with energy in eV.

3.7. Scanning electron microscopy (SEM)

SEM study was performed to evaluate their morphological properties in films before and after annealing. The SEM images of cNDI-1EHA, cNDI-2EHA, cNDI-3EHA and cNDI-4EHA before and after annealing (performed at 170 °C for 30 min) (FIg. 6) clearly shows difference in self-assembling behaviour. Sheet-like assembled structures of micrometer size can be clearly seen for all the three samples, due to interaction of aliphatic long alkyl chains on both the diimide position as well as core-substitutions. The SEM images after annealing show clear difference in morphology. cNDI-3EHA attains more crystallinity as compared to cNDI-1EHA and cNDI-2EHA show less packed structures. cNDI-4EHA is more hydrophobic and highly packed films due to excimer formation and strong π–π stacking. The cNDI-3EHA molecule bearing two alkyl chains on diimide position and three alkyl chains on core allow to arrange the molecule in well-ordered arrangement. Thus, based on SEM images, we obtained assembled in following ordered cNDI-1EHA<cNDI-4EHA<cNDI-2EHA<cNDI-3EHA and comparable to report of Wasielewski[59] and Govindraju.[60]

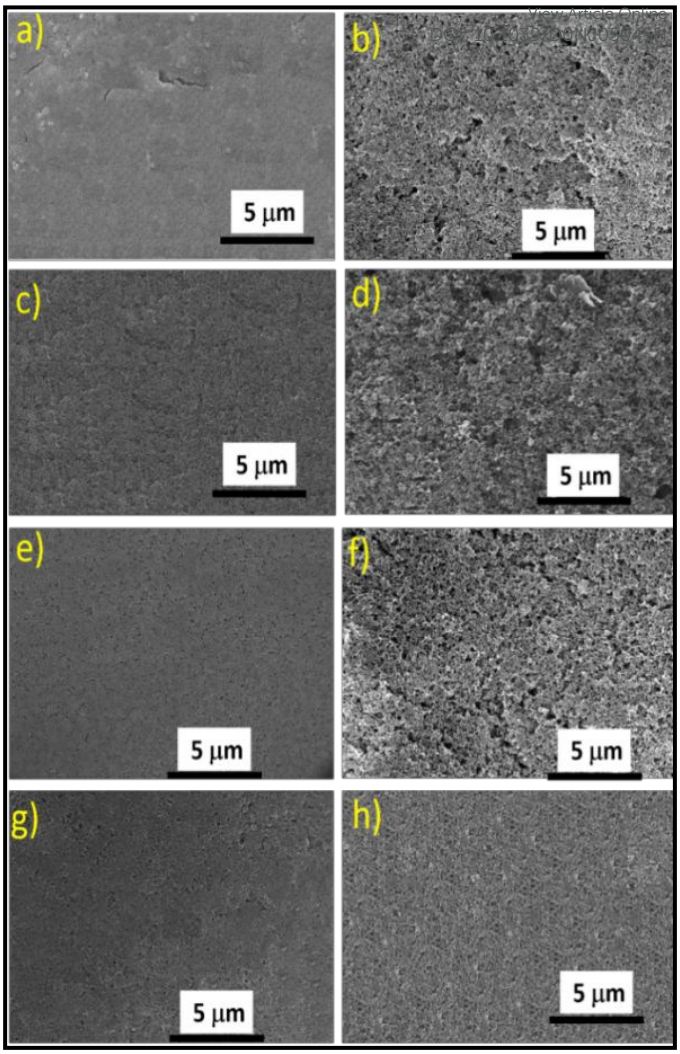

Fig. 6 SEM images for cNDI-1EHA, cNDI-2EHA, cNDI-3EHA and cNDI-4EHA before annealing (a, c, e and g); after annealing (performed at 170 °C for 30 min)(b, d, f and h), respectively.

3.8. X-ray diffraction characteristics

To further investigate the crystalline nature, we obtained high power X-ray diffraction (XRD) patterns for all the four cNDI-1EHA, cNDI-2EHA, cNDI-3EHA and cNDI-4EHA as casted thin film on Si-wafer see ESI FIg.S23. It can be seen that all four molecules showing broad peaks which is evident of the formation of ordered but non-crystalline file. However, after annealing of the film of four samples at performed at 170 °C for 30 min, showing the peaks lamellar d-spacing thin film at 2.4° found to be 8.17Å along with broad peak at 6.17 Å for cNDI-1EHA, 5.83 Å for cNDI-2EHA and 4.62 Å for cNDI-4EHA with increasing 2θ values with increase in substituted chain number cNDI-1EHA>cNDI-2EHA> cNDI-4EHA. Interestingly these broad peak missing in the case of cNDI-3EHA, suggesting that the thin film after annealing in the case of cNDI-3EHA exhibit completely different properties. Nevertheless, cNDI-1EHA, cNDI-2EHA and cNDI-4EHA also have broad peaks at 17.52 nm, however, cNDI-3EHAshows very sharp peaks 2θ > 7.2°. This XRD study also clearly supports our earlier hypothesis from SEM (FIg. 5) images, that cNDI-3EHA is self-assembled better crystalline in nature than that of other cNDI-1EHA, cNDI-2EHA and cNDI-4EHA derivatives.

View Article Online
DOI: 10.1039/D0NJ05045H

As illustrated in FIg. 7, based on SEM images (Fig. 6e and g and Fig. 6f and h) we presume the plausible molecular arrangement of cNDI-3EHA and cNDI-4EHA as film cased and after annealing 170 °C for 30 min.

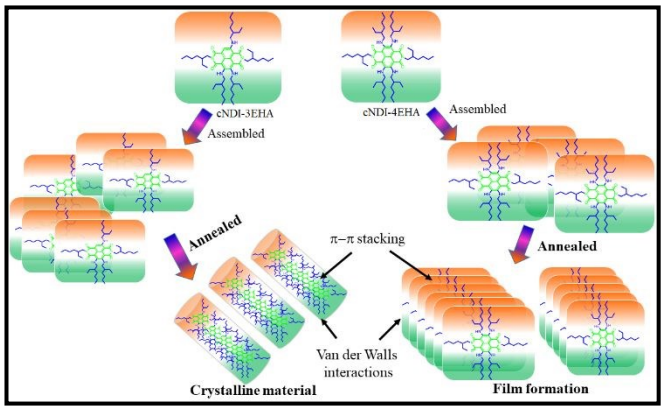

Fig. 7 Schematic presentation of cNDI-3EHA and cNDI-4EHA chromophores before annealing assembled into random structures for both of the molecules, however, after annealing, cNDI-3EHA produces crystalline assembly and cNDI-4EHA thin film, respectively.

3.9. Charge transport properties

To examine the influence of number and position of 2-ethyl-1-hexylamine chain on n-type semiconducting properties, we evaluated the electron mobility of these NDIs. The electron-only device (ITO/ZnO/NDIs/Al) based on cNDI-1EHA, cNDI-2EHA, cNDI-3EHA and cNDI-4EHA were fabricated and electron mobility was calculated. The electron mobility was determined by using the most versatile space charge limited current (SCLC) model for organic semiconductor materials.[42,49,61] As can be seen in Fig. 8a&b, the single carrier devices have been fabricated by sandwiching the NDI layer between contacts of different work functions so as to allow only one type of charge carriers selectively due to band-edge mismatch. The potential barrier at the interface of ZnO (7.4 eV) and ITO (4.8 eV) blocks the hole injection from ITO to NDI layer and only electrons are expected to flow.

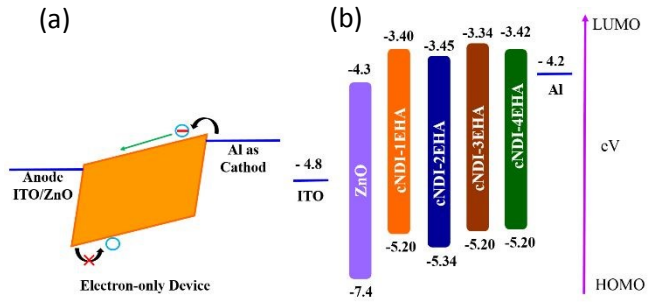

Fig. 8 Schematic representation of fabricated electron only device with energy level diagram of corresponding layers.

At room temperature, the space charge limited current shows quadratic dependency on voltage. The electron mobility of the NDI materials were extracted from the Mott-Gurney Eq. (1).

$$J = \frac{9}{8}\mu\epsilon\frac{V^2}{L^3}$$

Where J is the current density, L is the thickness of the organic semiconductor layer, μ is the mobility of organic semiconductor, ϵ is the permittivity of medium, and V is applied voltage.

The dark log(J)-log(V) curves for NDI chromophores-based electron only devices are illustrated in Fig. 9 and the electron mobility data are summarized in Table 2 and Table S1. Slope (i) and slope (ii) shows the Ohmic and SCLC regions respectively (Fig. 9). The cNDI-1EHA, cNDI-2EHA, cNDI-3EHA and cNDI-4EHA molecules in ITO/ZnO/NDIs (~100 nm)/Ag device exhibited electron mobility as high as 1.14×10^{-6} cm²/Vs, 1.25×10^{-4} cm²/Vs, 2.69×10^{-4} cm²/Vs and 1.4×10^{-6} cm²/Vs, respectively (FIg. 8 and Table 2). The electron mobility in case of NDI-2EHA and NDI-3EHA are higher than that of NDI-1EHA and NDI-4EHA, suggesting that the number and position of 2-ethyl-1-hexylamine chain play important role. The electron mobility trend not depends on number of chain length rather formation of crystalline material after annealing that is in the order cNDI-1EHA<cNDI-4EHA<cNDI-2EHA<cNDI-3EHA. The highest electron mobility value was observed with cNDI-3EHA. From XRD data (FIg. S23) and SEM (FIg. S24) images is clear that cNDI-3EHA produces very good crystalline morphologies have better electron mobility.

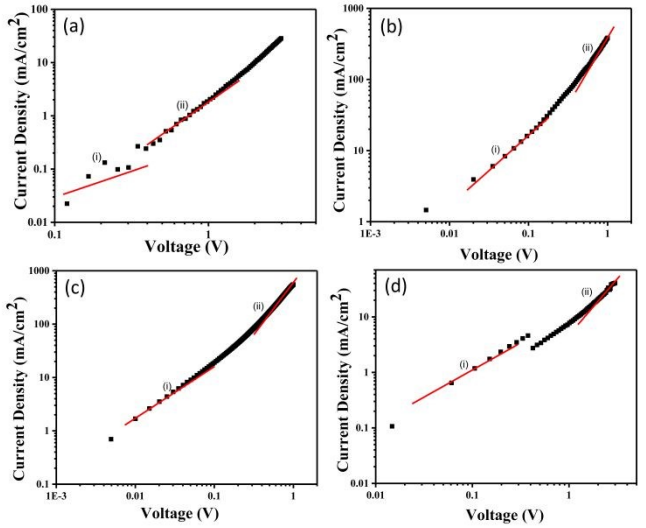

Fig. 9 Electron mobility of (a) cNDI-1EHA, (b) cNDI-2EHA, (c) cNDI-3EHAand cNDI-4EHA. The device architecture is ITO/ZnO/NDIs/Al. The red lines show slope for ohmic (i) and SCLC regions (ii) respectively.

View Article Online
DOI: 10.1039/D0NJ05045H

Table 2: Best optimized condition for electron mobility properties of cNDI-1EHA, cNDI-2EHA, cNDI-3EHA and cNDI-4EHA.

Sample Code	Concentration (Chlorobenzene)	Annealing Temp.	Device Structure	e-mobility (cm^2/Vs)
cNDI-1EHA	40 mg/mL	170°C	ITO/ZnO/ cNDI-1EHA/Al	$1.14x10^{-6}$
cNDI-2EHA	40 mg/mL	170°C	ITO/ZnO/ cNDI-2EHA/Al	$1.25x10^{-4}$
cNDI-3EHA	40 mg/mL	170°C	ITO/ZnO/ cNDI-3EHA/Al	$2.69x10^{-4}$
cNDI-4EHA	40 mg/mL	170°C	ITO/ZnO/ cNDI-4EHA/Al	$1.4x10^{-6}$

The electron mobility results obtained from this work is compared with the literature report on the electron mobility performance of naphthalene diimide based small molecules by SCLC method and are summarized in Table 3. The results display the comparative electron mobility performance in this work compared to the literature report.

Table 3: Literature reports on the performance of NDI based small molecules for electron mobility characteristics with SCLC method.

Structures	Electron Mobility $cm^{-1}\ V^{-1}\ s^{-1}$	Device Structure	Reference
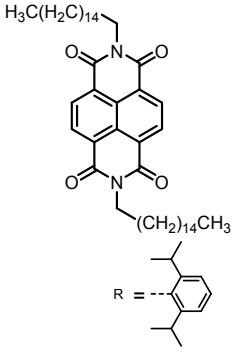	1.8×10^{-3}	ITO/ZnO/ NDI derivative (200 nm)/Al	49
	4.17×0^{-3}		
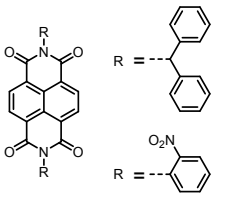	2.16×0^{-3}	ITO/ZnO/ NDI derivatives (200 nm)/Al	42
	2.5×10^{-5}		
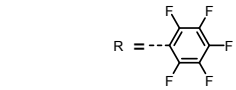	7.9×10^{-4}		
	$6.08 \pm 1.13 \times 10^{-5}$	ITO/ZnO/ NDI derivatives (5-10 μm)/Al	62
	$4.50 \pm 3.03 \times 10^{-4}$		
	$9.04 \pm 5.25 \times 10^{-8}$		
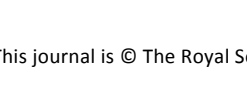	$1.28 \pm 1.32 \times 10^{-3}$		
	1.14×10^{-6}	ITO/ZnO/ NDI derivative (40 mg/mL)/Al	This work
	1.25×10^{-4}		
	2.69×10^{-4}		
	1.4×10^{-6}		

4. Conclusions

In conclusion, we have synthesized four naphthalenediimide (NDI) derivatives through core-substitution with varying number of 2-ethyl-hexylamine (EHA) substituents at different positions and studied their optical, self-assembling, electronic and charge transport properties. The absorption measurement reveals that the increase in number of 2-ethyl-1-hexylamine substituent at NDI core showed longer λ_{max}^{onset} and displays strong ICT transition, resulting significant decrease in optical band gap. Electrochemical analysis shows the low-lying LUMO energy level as required for stable n-type OSCs. The SEM and XRD analysis clearly illustrates thatcNDI-3EHA gives more crystallinity than the other three NDI derivatives showing strong π–π-stacking and van der Walls interactions within the aggregated stacks that play a major role in arrangement of molecules in directional growth. Further, the electron mobility of the materials has also been evaluated which is in the range of 10^{-4} to 10^{-6} cm^2/Vs, clearly indicate that number and position of 2-ethyl-1-hexylamine chain play effective role in electron transport due to ordered film formation. The excellent electrical and optical properties of these materials make them a promising n-type material for wide applications in various semiconducting devices.

Conflicts of interest

"All authors declare there are no conflicts of interest".

Acknowledgements

S.V.B. (IICT) is grateful for financial support from the DAE-BRNS Project Code: 58/14/01/2020-BRNS/37047, Mumbai, India.

IICT/Pubs./2020/191.S. V. B. (GU) acknowledges financial support from the UGC-FRP programme. S.S.B. is grateful for financial support from CSIR, New Delhi for SRF fellowship. Dedicated to Prof. Jürgen-Hinrich Fuhrhop on the occasion of his 80th Birthday

Notes and references

1 H. Sirringhaus, *Adv.Mater.,*2014, **26**, 1319-1335.

2 (a) P. F. Van Hutten, V. V. Krasnikov and G. Hadziioannou, *Acc. Chem. Res*., 1999, **32**, 257-265; (b) Y. Watanable, H. Sasabe, and *J.* Kido, *Bull. Chem. Soc. Jpn.* 2019, **92**, 716-728; (c) J.-H. Lee, C.-H. Chen, P.-H. Lee, H.-Y. Lin, M.-k. Leung, T.-L. Chiu, and C.-F. Lin, *J. Mater. Chem. C,* 2019, **7**, 5874—5888

3 C. Brabec, U. Scherf and V. Dyakonov, *Organic Photovoltaics: Materials, Device Physics, and Manufacturing Technologies*, 2nd ed.; Wiley: Hoboken, NJ, 2016**.**

4 J. E. Anthony, A. Facchetti, M. Heeney, S. R. Marder and X. Zhan, *Adv. Mater.,* 2010**, 22**, 3876-3892.

5 A. Facchetti, *Mater. Today,* 2007, **10**, 28-37.

6 K.-J. Baeg, M. Caironi and Y.-Y. Noh, *Adv. Mater*., 2013, **25**, 4210-4244.

7 C.-a. Di, F. Zhang and D. Zhu, *Adv. Mater*., 2013, **25**, 313-330.

8 H. Li, W. Shi, J. Song, H.-J. Jang, J. Dailey, J. Yu and H. E. Katz, *Chem. Rev.,* 2019, **119**, 3-35.

9 J.Zaumesil and H. Sirringhaus, *Chem. Rev.,* 2007, **107**, 1296-1323.

10 J. Zhang, J. Jin, H. Xu, Q. Zhang and W.Huang, *J. Mater. Chem. C*, 2018, **6**, 3485 – 3498.

11 H. E. Katz, A. J. Lovinger, J. Johnson, C. Kloc, T. Siegrist, W. Li, Y. Lin and A. Dodabalapur, *Nature,*2000, **404**, 478-481.

12 C. R. Newman, C. D. Frisbie, D. A. S. Filho, J. L. Brédas, P. C. Ewbank And K. R. Mann,*Chem. Mater.*,2004, **16**, 4436-4451.

13 A. Maliakal, *In Organic Field-Effect Transistors;* Z. Bao, J. Locklin, CRC Press: Boca Raton, FL, 2007; p 229.

14 Y. Shirota and H. Kageyama, *Chem. Rev.,* 2007, **107**, 953-1010.

15 C. Wang, H. DongW. Hu, Y. Liu and D. Zhu, *Chem. Rev.,* 2012, **112**, 2208-2267.

16 B. A. Jones, A.Facchetti, M. R. Wasielewski and T. J. Marks, *J. Am. Chem. Soc.,* 2007*,* **129***,* 15259– 15278*.*

17 K. Iijima, Y. L. Gal, T. Higashino, D. Lorcy and T. Mori, *J. Mater. Chem. C*, 2017, **5**, 9121-9127.

18 K. Iijima, Y. L. Gal, D. Lorcy and T. Mori, *RSC Adv.,*2018, **8**, 18400-18405.

19 S.Naqvi, N.Vasishtha, M.Kumar and R. Kumar, *New J. Chem.,* 2019, **43**, 15626--15635.

20 S. Naqvi, N. Gupta, N.Kumari, J. Garg, R. Kumar, *New J. Chem*., **2017**, *41*, 1933-1939.

21 Y. Wang, T. Hasegawa, H. Matsumoto, T. Mori and T. Michinobu, *Adv. Mater.,* 2018, **30**, 1707164.

22 T. Hasegawa, M. Ashizawa, K. Aoyagi, H. Masunaga, T. Hikima and H. Matsumoto, *Org. Lett.,* 2017, **19**, 3275-3278.

23 Y. Qiao, Y. Guo, C. Yu, F. Zhang, W. Xu, Y. Liu and D. Zhu, *J. Am. Chem. Soc.,* 2012, **134**, 084-4087.

24 K. Iijima and T. Mori, *Chem. Lett.,* 2017, **46**, 357-359.

25 T. Lei, Y. Cao, Y. Fan, C.-J. Liu, S.-C. Yuan and J. Pei, *J. Am.Chem. Soc*.,2011, **133**, 6099-6101.

26 R. Stalder, J. Mei, K. R. Graham, L. A. Estrada and J. R. Reynolds, *Chem. Mater.,*2014, **26**, 664-678.

27 D. Yoo, X. Luo, T. Hasegawa, M. Ashizawa, T. Kawamoto, H. Masunaga, N. Ohta, H. Matsumoto, J. Mei and T. Mori, *ACS Appl. Electron. Mater.,*2019, **1**, 764-771.

28 X. Zhan, A. Facchetti, S. Barlow, T. J. Marks, M. A. Ratner, M. R. Wasielewski and S. R. Marder, *Adv. Mater.*, 2011, **23**, 268-284.

29 G. C. Schmidt, D.Höft, K. Haase, A. C. Hübler, E. Karpov, R. Tkachov, M. Stamm, A. Kiriy, F. Haidu, D. R. T. Zahn, H. Yan and A. Facchetti, *J. Mater. Chem. C,* 2014, **2**, 5149-5154

30 R. Pfattner, C. Rovira and M. Mas-Torrent, *Phys. Chem. Chem. Phys.,* 2015, **17**, 26545-26552.

31 W. Liu, D.B. Shaikh, P. S. Rao, R. S. Bhosale, A. A. Said, A. M. Mak, Z. Wang, M. Zhao, W. Gao, B. Chen, Y. M. Lam, W. Fan, S. V. Bhosale, S. V. Bhosale and Q. Zhang, *Chem. Asian J.,* 2020, **15**, 112-121.

32 D. B. Shaikh, A. Said, R. S. Bhosale, W. Chen, S.V. Bhosale, A. L. Puyad, S. V. Bhosale and Q. Zhang, *Asian J. Org. Chem*., 2018, **7**, 2294-2301.

33 A. A. Said, S. M. Wagalgave, J. Xie, A. L. Puyad, W. Chen, Z. Wang, S. V. Bhosale, S. V. Bhosale and Q. Zhang, *J. Solid State Chem.,*2019, **270**, 51-57.

34 S. Peng, J. Miao, I. Murtaza, L. Zhao, Z. Hu, M. Liu, T. Yang, Y. Liang, H. Meng and A. W. Huang, *J. Mater. Chem. C,* 2017, **5**, 5949-5955.

35 J. Miao, Z. Hu, M. Liu, M. U. Ali, O. Goto, W. Lu, T. Yang, Y. Liang and H. Meng, *Org. Electron.,*2018, **52**, 200-205.

36 S. Naqvi, M.Kumar and R. Kumar, *ACS Omega,* 2019, **4**, 19735-19745 and the references cited herein.

37 J. H. Oh, S.-L. Suraru, W.-Y. Lee, M. Könemann, H. W. Höffken, C. Röger, R. Schmidt, Y. Chung, W.-C. Chen, F. Würthner and Z. Bao, *Adv. Funct. Mater.,* 2010, **20**, 2148-2156.

38 J. G. Laquindanum, H. E. Katz, A. Dodabalapur and A. J. Lovinger, *J. Am. Chem. Soc.,* 1996, **118**, 11331-11332.

39 J. Chang, Q. Ye, W. K. Huang, J. Zhang, K. J. Chen and J. Wu, C. Chi *Org. Lett.,* 2012, **14**, 2964-2967.

40 X. Chen, Y. Guo, L. Tan, G. Yang, Y. Li, G. Zhang, Z. Liu, W. Xu and D. Zhang, *J.Mater. Chem. C,* 2013, **1**, 1087-1092.

41 J. Chang, J. Shao, J. Zhang, J. Wu and C. Chi, *RSC Adv*., 2013, **3**, 6775-6778.

42 N. Kumari, S. Naqui, M. Ahuja, K. Bhardwaj and R. Kumar, *J. Mater. Sci.: Mater. Electron*.,2020, **31**, 4310–4322.

43 A. Dey, A. Kalita and P. K. Iyer, *ACS Appl. Mater. Interfaces*,2014, **6**, 12295-2301.

44 T. He, M. Stolte and F. Würthner, *Adv. Mater.*,2013, **25**, 6951-6955.

45 X. Gao, C.-a. Di, Y. Hu, X. Yang, H. Fan, F. Zhnag, Y. Liu, H. Li and D. Zhu, *J. Am. Chem. Soc.,*2010, **132**, 3697-3699.

46 H. Yan, Z. Chen, Y. Zheng, C. Newman, J. R. Quinn, F. Dötz, M. Kastler and A. Facchetti, *Nature,*2009, **457**, 679-687.

47 W.-Y. Lee, J. H. Oh, S.-L. Suraru, W.-C. Chen, F. Würthner and Z. Bao, *Adv. Funct. Mater.,*2011, **21**, 4173-4181.

48 F. Zhang, Y. Hu, T. Schuettfort, C.-A. Di, X. Gao, C.R. McNeill, L. Thmsen, S. C. B. Mannsfeld, W. Yuan, H. Sirringhaus and D. Zhu, *J. Am. Chem. Soc.,*2013, **135**, 2338-2349

49 N. Kumari, S. Naqui and R. Kumar, *J. Mater. Sci.,* 2018, **53**, 4046-4055.

50 (a) R. Fernando, F. S. Etheridge, E. Muller and Sauve, *New J. Chem.* 2015, **39***,* 2506-2514; (b) R. Fernando, Z. Mao and G. Sauvé*, Org. Electron*.,2013, **14**, 1683-1692; (c) G. Sauvé,*Chem. Rec.,* 2019,**19**, 1-16.

51 X. Guo, F. S. Kim, M. J. Seger, S. A. Jenekhe andM. D. Watson, *Chem. Mater.,*2012, **24**, 1434–1442 and references cited herein.

52 Z. Ma, H. Geng, D. Wangand Z. Shuai, *J. Mater. Chem. C,*2016, **4**, 4546-4555.

53 A. Welford, S. Maniam, E. Gann, X. Jiao, L. Thomsen and S. J. Langford, C. R. McNeill, *Org. Electron.,* 2019, **75**, 105378.

54 (a) M. Sasikumar, Y.V. Suseela and T.Govindaraju, *Asian J. Org. Chem.,*2013, **2**, 779-785; (b) X. Gao, W. Qiu, X. Yang, Y. Liu, Y. Wang, H. Zhnag, T. Qi, Y. Liu, K. Lu, C. Du, Z. Shuai, G. Yu, and D. Zhu, *Org. Lett*., 2007, **9**, 3917-3920

55 Gaussian 09, Revision C.01 M. J. Frisch, G. W. Trucks, H. B. Schlegel, G. E. Scuseria,M. A. Robb, J. R. Cheeseman, G. Scalmani, V. Barone, B. Mennucci, G. A. Petersson, H. Nakatsuji, M. Caricato, X. Li, H. P. Hratchian, A. F. Izmaylov, J. Bloino, G. Zheng, J. L. Sonnenberg, M. Hada, M. Ehara, K. Toyota, R. Fukuda, J. Hasegawa, M. Ishida, T. Nakajima, Y. Honda, O. Kitao, H. Nakai, T. Vreven, J. A. Montgomery, Jr., J. E. Peralta, F. Ogliaro, M. Bearpark, J. J. Heyd, E. Brothers, K. N. Kudin, V. N. Staroverov, T. Keith, R. Kobayashi, J. Normand, K. Raghavachari, A. Rendell, J. C. Burant, S. S. Iyengar, J. Tomasi, M. Cossi, N. Rega, J. M. Millam, M. Klene, J. E. Knox, J. B. Cross, V. Bakken, C. Adamo, J. Jaramillo, R. Gomperts, R. E. Stratmann, O. Yazyev, A. J. Austin, R. Cammi, C. Pomelli, J. W. Ochterski, R. L. Martin, K. Morokuma, V. G. Zakrzewski, G. A. Voth, P. Salvador, J. J. Dannenberg, S. Dapprich, A. D.

View Article Online
DOI: 10.1039/D0NJ05045H

Daniels, O. Farkas, J. B. Foresman, J. V. Ortiz, J. Cioslowski, and D. J. Fox, Gaussian, Inc., Wallingford CT, 2010.
56 N.M. O'Boyle, A.L. Tenderholt and K.M. Langner, *J. Comp. Chem.,*2008, **29**, 839-845.
57 Avogadro: *an open-source molecular builder and visualization tool. Version 1.1.0*. http://avogadro.openmolecules.net/
58 M. D. Hanwell, D. E. Curtis, D. C. Lonie, T. Vandermeersch, E. Zurek and G. R. Hutchison, *J. Cheminformatics,* 2012, **4***,* 17.
59 M.R. Wasielewski, *Acc. Chem. Res.*, 2009, **42**, 1910–19201.
60 M.B. Avinash and T. Govindraju, *Adv. Funct. Mater.,* 2011, **21**, 3875–3882.
61 J. C. Blakesley, F. A. Castro, W. Kylberg, G. F.A. Dibb, C. Arantes, R. Valaski, M. Cremona, J.S. Kim and J. -S. Kim, *Org. Electron.,*2014, **15**, 1263-1272.
62 M. B. Avinash, K. Swathi, K. S. Narayan, and T. Govindaraju, *ACS Appl. Mater. Interfaces,* 2016, **8,** 8678−8685.

View Article Online
DOI: 10.1039/D0NJ05045H

Graphical Abstract